NASA TECHNICAL MEMORANDUM

NASA TM X-71472

NASA TM X-71472

APPLICATION OF BOUNDARY INTEGRAL METHOD TO ELASTOPLASTIC ANALYSIS OF V-NOTCHED BEAMS

by Walter Rzasnicki and Alexander Mendelson
Lewis Research Center
Cleveland, Ohio 44135

TECHNICAL PAPER proposed for presentation at
Seventh U.S. National Congress of Applied Mechanics sponsored by the
U.S. National Committee of Theoretical and Applied Mechanics of the
National Academy of Sciences
Boulder, Colorado, June 3-7, 1974

APPLICATION OF BOUNDARY INTEGRAL METHOD TO ELASTOPLASTIC ANALYSIS OF V-NOTCHED BEAMS

by Walter Rzasnicki and Alexander Mendelson*
Lewis Research Center
National Aeronautics and Space Administration
Cleveland, Ohio

SUMMARY

The boundary integral equation method was applied in the solution of the plane elastoplastic problems. The use of this method was illustrated by obtaining stress and strain distributions for a number of specimens with a single edge notch and subjected to pure bending. The boundary integral equation method reduced the non-homogeneous biharmonic equation to two coupled Fredholm-type integral equations. These integral equations were replaced by a system of simultaneous algebraic equations and solved numerically in conjunction with the method of successive elastic solutions.

E-7658

INTRODUCTION

Knowledge of the stress distribution in the neighborhood of a singularity, such as the tip of a V-notch in a bar loaded in tension or bending, is of fundamental importance in evaluating the resistance to fracture of structural materials. Elastic solutions to various geometries have been obtained by a number of different methods. Among the more effective ones, are the complex variable method (ref. 1), collocation method (ref. 2),

* Submitted to the International Journal of Fracture Mechanics.

and finite element method (ref. 3). However, the first two of these methods are not general enough nor readily adaptable to three-dimensional or elastoplastic problems. And the finite element method requires solutions of large sets of equations and fails to give sufficiently fine resolution in the vicinity of notch tips.

The recently developed boundary integral methods (ref. 4) offer an attractive alternative to other methods of analysis. These methods have a number of advantages as listed in references 4 and 5, the most important of which is that nodal points are needed only on the boundary instead of throughout the region as required by finite element methods. To date these methods have been used primarily for obtaining elastic solutions to various problems. Their extension to elastoplastic problems has been proposed in references 4 and 6. However no elastoplastic solution has heretofore been obtained.

The present paper describes the application of a boundary integral method to the solution of the elastic and elastoplastic problems of a V-notched beam in pure bending. Solutions of such problems for the elastoplastic case by finite elements has not been too successful in obtaining fine enough resolution and sufficiently accurate results in the vicinity of the notch tip (ref. 7). The present method overcomes these difficulties,

since the stress and strain can be computed at any arbitrary point in the body from a knowledge of boundary values only.

METHOD OF SOLUTION

The problem of determining the state of stress and strain in a plane elastoplastic problem can be reduced to solving the following non-homogeneous biharmonic equation for the Airy stress function, as shown in reference 8:

$$\nabla^4 \Phi = g(x,y) \tag{1}$$

$$g(x,y) = -\frac{E}{1-\mu^2}\left[\frac{\partial^2}{\partial y^2}(\varepsilon_x^p + \Delta\varepsilon_x^p) + \frac{\partial^2}{\partial x^2}(\varepsilon_y^p + \Delta\varepsilon_y^p) - 2\frac{\partial^2}{\partial x \partial y}(\varepsilon_{xy}^p + \Delta\varepsilon_{xy}^p)\right] + \frac{\mu E}{1-\mu^2}\nabla^2(\varepsilon_x^p + \Delta\varepsilon_x^p + \varepsilon_y^p + \Delta\varepsilon_y^p) \tag{2}$$

for the plane strain case, and

$$g(x,y) = -E\left[\frac{\partial^2}{\partial y^2}(\varepsilon_x^p + \Delta\varepsilon_x^p) + \frac{\partial^2}{\partial x^2}(\varepsilon_y^p + \Delta\varepsilon_y^p) - 2\frac{\partial^2}{\partial x \partial y}(\varepsilon_{xy}^p + \Delta\varepsilon_{xy}^p)\right] \tag{3}$$

for the plane stress case, where ε_x^p, ε_y^p, and ε_{xy}^p represent the accumulation of plastic strain increments from the beginning of the loading history up to, but not including the current

increment of the load, and $\Delta\varepsilon_x^p$, $\Delta\varepsilon_y^p$, and $\Delta\varepsilon_{xy}^p$ are the increments of plastic strain due to the current increment of load. For the elastic case, $g(x,y)$ is of course equal to zero.

The stress function φ must satisfy appropriate boundary conditions. For the problem under consideration (fig. 1) $\varphi(x,y)$ and its outward normal derivative $\partial\varphi/\partial n$ must satisfy the following boundary conditions (ref. 9):

$$\left.\begin{aligned}
&\text{along boundary OA and OA'} \quad \varphi(x,y) = 0; \ \frac{\partial\varphi}{\partial n} = 0 \\
&\text{along boundary AB and A'B'} \quad \varphi(x,y) = 0; \ \frac{\partial\varphi}{\partial n} = 0 \\
&\text{along boundary BC and B'C'} \\
&\varphi(x,y) = -\frac{\sigma_{max}}{w}\left(\frac{x^3}{3} + ax^2 + a^2x + \frac{a^3}{3}\right) + \sigma_{max}\left(\frac{x^2}{2} + ax + \frac{a^2}{2}\right) \\
&\frac{\partial\varphi}{\partial n} = 0 \\
&\text{along boundary CD and C'D} \quad \varphi(x,y) = \frac{\sigma_{max} w^2}{6}; \ \frac{\partial\varphi}{\partial n} = 0
\end{aligned}\right\} \quad (4)$$

To solve equation (1) by means of the boundary integral method use is made of Green's second theorem to reduce this equation to coupled integral equations, as shown in references 4 and 9. The result is

$$8\pi\Phi(x,y) - \int\int_R \rho g(\xi,\eta)\,d\xi d\eta = \int_C \left[\Phi \frac{\partial}{\partial n}(\nabla^2 \zeta) - \frac{\partial \Phi}{\partial n}\nabla^2\rho + \phi \frac{\partial \rho}{\partial n} - \frac{\partial \phi}{\partial n}\rho\right] ds \quad \text{for } P \subset R \tag{5}$$

$$4\pi\Phi(x,y) - \int\int_R \rho g(\xi,\eta)\,d\xi d\eta = \int_C \left[\Phi \frac{\partial}{\partial n}(\nabla^2 \rho) - \frac{\partial \Phi}{\partial n}\nabla^2\rho + \phi \frac{\partial \rho}{\partial n} - \frac{\partial \phi}{\partial n}\rho\right] ds \quad \text{for } P \subset C \tag{6}$$

and

$$2\pi\phi(x,y) - \int\int_R g(\zeta,\eta) \ln r\, d\xi d\eta = \int_C \left[\phi \frac{\partial}{\partial n}(\ln r) - \frac{\partial \phi}{\partial n} \ln r\right] ds \quad \text{for } P \subset R \tag{7}$$

$$\pi\Phi(x,y) - \int\int_R g(\xi,\eta)\ln r \, d\xi d\eta =$$

$$\int_C \left[\Phi \frac{\partial}{\partial n} (\ln r) - \frac{\partial \Phi}{\partial n} \ln r \right] ds \quad \text{for } P \in C \qquad (8)$$

where

$\Phi \equiv \nabla^2 \varphi$

$\rho \equiv r^2 \ln r$

and

$r(x,y;\xi,\eta)$ is the distance between any two points $P(x,y)$ and $q(\xi,\eta)$ or $P(x,y)$ and $Q(\xi,\eta)$, as shown in figure 2.

Equation (5) would, for a known function $g(x,y)$, give us directly a solution to the biharmonic equation (1) provided the functions $\varphi(x,y)$, $\partial\varphi(x,y)/\partial n$, $\nabla^2\varphi(x,y)$ and $\partial[\nabla^2\varphi(x,y)]/\partial n$ were known on the boundary C.

However, only the stress function φ and its outward normal derivative $\partial\Phi/\partial n$ are specified (eq. (4)). The values of $\nabla^2\varphi \equiv \Phi$ and $\partial(\nabla^2\varphi)/\partial n \equiv \partial\Phi/\partial n$ on the boundary must be compatible with the given values of Φ and $\partial\Phi/\partial n$. To assure this compatibility, we have to solve the system of coupled

integral equations (6) and (8), which contain the unknown functions Φ and $\partial\Phi/\partial n$.

Once the values of Φ and $\partial\Phi/\partial n$ on the boundary C of region R are known we can proceed with the calculation of the stress field in the region R utilizing equation (5) and the equations which define φ, namely

$$\sigma_x = \partial^2\varphi/\partial y^2,\ \sigma_y = \partial^2\varphi/\partial x^2\ \sigma_{xy} = -\partial^2\varphi/\partial x\partial y \qquad (9)$$

The calculation of the function $g(x,y)$ which is obtained iteratively, is discussed in detail in reference 9.

NUMERICAL PROCEDURES

Solution of the Integral Equations

Since it is generally impossible to solve the system of coupled integral equations analytically, a numerical method is utilized in which the integral equations (6) and (8) are replaced by a system of simultaneous algebraic equations.

For simplicity of notation the normal derivatives are denoted by prime superscripts. The boundary is divided into n intervals, not necessarily equal, numbered consecutively in the direction of increasing s. The center of each interval is designated as a node. The values of Φ and Φ' are assumed constants on each interval and equal to the values calculated at the node.

In a similar manner the interior of region R is covered by a grid, containing m cells. The cells do not have to have equal areas. Their nodal points are located at the centroids. The value of $g(\xi,\eta)$ is assumed constant over each cell and equal to the value calculated at the centroid.

The arrangements of boundary and interior region sub-divisions is shown in figures 3 and 4. Using the above assumptions, equations (6) and (8) can be replaced by a system of 2n simultaneous algebraic equations with 2n unknowns, that is, Φ_i and Φ_i'

$$\left.\begin{aligned} \pi\Phi_i - \sum_{k=1}^{m} \ln r_{ik}(gA)_k &= \sum_{j=1}^{n} (a_{ij}\Phi_j + b_{ij}\Phi_j') \\ 4\pi\varphi_i - \sum_{k=1}^{m} \rho_{ik}(gA)_k &= \sum_{j=1}^{n} (c_{ij}\Phi_j + d_{ij}\Phi_j' + e_{ij}\varphi_j + f_{ij}\varphi_j') \end{aligned}\right\} \quad (10)$$

where $i = 1,2,3\ldots n$, r_{ik} is the distance from i^{th} node to the centroid of the k^{th} cell, A_k is the area of the k^{th} cell, and

$$
\left.
\begin{aligned}
a_{ij} &= \int_j (\ln r_{ij})' \, ds \\
b_{ij} &= -\int_j \ln r_{ij} ds \\
c_{ij} &= \int_j \rho'_{ij} ds \\
d_{ij} &= -\int_j \rho_{ij} ds \\
e_{ij} &= \int_j (\nabla^2 \rho_{ij})' ds \\
f_{ij} &= -\int_j \nabla^2 \rho_{ij} ds
\end{aligned}
\right\} \qquad (11)
$$

where integration is taken over the j^{th} interval, and r_{ij} is the distance from i^{th} node to any point in the j^{th} interval. The normal derivatives in equations (11) are taken on the j^{th} interval.

For curved boundaries the coefficients given by equations (11) can be evaluated, if necessary, by Simpson's rule for $i \neq j$. For $i = j$, because of the singular nature of the integrand, the integrals for the coefficients must be evaluated by a limiting process. For boundary intervals, such as for the problem treated herein,

which can be represented by straight lines a closed form solution can be obtained for these coefficients (ref. 9).

Boundary equations (10) can be written in matrix form as

$$[B]\{X\} = \{R\} \tag{12}$$

where [B] is 2n x 2n matrix and $\{X\}$ and $\{R\}$ are 2n x 1 column matrices.

Matrix [B] is dependent only on geometry, that is, number of nodes and their distribution on the boundary. Since the matrix $\{R\}$ contains the nonlinear function $g(\xi,\eta)$, which depends on the stress field and therefore on matrix $\{X\}$, and iterative process will be used to obtain the solution.

To calculate stresses, at any nodal point in the region R, from the stress function Φ we need not perform any numerical differentiation. Equation (5) can be differentiated under the integral sign and once Φ and Φ' are known on the boundary the stresses can be obtained by the same type of numerical integration as in equations (10). Applying equations (9) to equation (5) yields for the case of a rectangular grid the following stress equations:

$$
\left.
\begin{aligned}
8\pi\sigma_{x,i} &= \left\{ \left[\ln \left(\frac{\delta_x^2 + \delta_y^2}{4} \right) + \frac{2\delta_y}{\delta_x} \tan^{-1} \frac{\delta_x}{\delta_y} - 1 \right] (gA) \right\}_{i=k} \\
&+ \sum_{k=1}^{m} \left\{ \ln[(x-\xi)^2 + (y-\eta)^2] + \frac{2(y-\eta)^2}{(x-\xi)^2 + (y-\eta)^2} + 1 \right\}_{ik} (gA)_k \qquad i \neq k \\
&+ \sum_{j=1}^{n} \left(A_{ij}\varphi_j + B_{ij}\varphi_j' + C_{ij}\Phi_j + D_{ij}\Phi_j' \right) \\
8\pi\sigma_{y,i} &= \left\{ \left[\ln \left(\frac{\delta_x^2 + \delta_y^2}{4} \right) + \frac{2\delta_x}{\delta_y} \tan^{-1} \frac{\delta_y}{\delta_x} - 1 \right] (gA) \right\}_{i=k} \\
&+ \sum_{k=1}^{m} \left\{ \ln[(x-\xi)^2 + (y-\eta)^2] + \frac{2(x-\xi)^2}{(x-\xi)^2 + (y-\eta)^2} + 1 \right\}_{ik} (gA)_k \qquad i \neq k \\
&+ \sum_{j=1}^{n} \left(-A_{ij}\varphi_j - B_{ij}\varphi_j' + E_{ij}\Phi_j + F_{ij}\Phi_j' \right) \\
-8\pi\sigma_{xy,i} &= \sum_{k=1}^{m} \left[\frac{2(x-\xi)(y-\eta)}{(x-\xi)^2 + (y-\eta)^2} \right]_{ik} (gA)_k \qquad i \neq k \\
&+ \sum_{j=1}^{n} \left(G_{ij}\varphi_j + H_{ij}\varphi_j' + I_{ij}\Phi_j + K_{ij}\Phi_j' \right)
\end{aligned}
\right\} \quad (13)
$$

where now i = 1,2,3...m and refers to the centroid of the i^{th} cell, δ_x and δ_y represent, respectively, x-directional and y-directional dimension of the cell. The coefficients A_{ij}, B_{ij}, C_{ij}, D_{ij}, E_{ij}, F_{ij}, G_{ij}, H_{ij}, I_{ij}, K_{ij} are obtained by appropriate differentiation under the integral sign of the coefficients given by equations (11) and are listed in reference 9.

Boundary Interval and Interior Grid Size

Use was made of the geometric and loading symmetry about the x axis for the problem treated herein to reduce the number of unknowns by approximately a factor of two. Since the vicinity of the notch tip is of greatest interest, a fine nodal spacing along the notch was chosen. However to maintain a reasonable number of nodal points, and at the same time to obtain fine resolution at the tip of the notch, the boundary along the notch was divided into a number of intervals progressively increasing in length as one moved away from the tip. The rate of change in the interval's length along this boundary was optimized by the method presented in reference 5. For the cases considered optimum ratios of the lengths of two consecutive boundary intervals were found to be in the range of 1.08 to 1.10. The resulting smallest dimensionless boundary interval length varied from 0.0001 to 0.0002. The nodal arrangement shown in figure 5

was used for all cases considered, resulting in a set of 140 equations containing 140 unknowns.

The choice of the size of the grid, which has to cover the region where plastic flow is expected to occur, is discussed in detail in reference 9. The smallest cells located in the vicinity of the tip of the notch have dimensions $\delta_x/w = 0.004$; $\delta_y/w = 0.008$ for plane strain cases, and $\delta_x/w = 0.004$, $\delta_y/w = 0.016$ for plane stress cases. A typical interior grid is shown in figure 5.

The solution to this boundary value problem is obtained by an iterative process, known as the method of successive elastic solutions described in detail in reference 8. This method, applied to the present problem, is presented in reference 9. Once the successive approximation procedure has converged, the stresses and strains are known everywhere in the beam.

RESULTS AND DISCUSSION

A number of beam problems were solved for both plane stress and plane strain cases. These included notch depth to beam depth ratios of 0.3 and 0.5, notch angles of 3° and 10°, strain hardening parameter values of 0.05 and 0.1. In addition calculations were performed using the actual stress-strain curve of a 5083-0 aluminum alloy in order to compare the calculated results for the crack opening displacements with available experimental

results. The detailed results for all cases are given in reference 9. Here, only a few typical results are presented.

Calculations were first made to check the method for the elastic problem, with the function g set equal to zero. For the elastic case a larger number of notch depths was used than for the elastoplastic case. A comparison with the boundary collocation results of reference 2 is shown in figures 6 to 8. Very good agreement was obtained.

The stress intensity factor K_I is here defined by

$$K_I = \lim_{r \to 0} \sqrt{2\pi}\, r^n \sigma_y(r,0) \tag{14}$$

Figures 9 to 12 show typical plastic zone growth with load for a plane strain case and for a plane stress case.

Variation of the dimensionless stress intensity factor with load is shown in figure 13 for the case of a specimen with notch depth of $a/w = 0.5$ and $\alpha = 10^{\circ}$, under plane strain condition and two values of strain hardening parameter m. It is to be noted that n appearing in equation (14) is no longer constant as in the elastic case, but is a function of the applied load. The stress intensity factor shows no significant increase over the linear elastic value up to an applied load of $q = \sigma_{max}/\sigma_0 = 0.40$. Above this load K_I increases progressively for both m's, at the faster rate for lower strain hardening parameter.

In order to verify in part, the numerically computed results, the notch opening displacements for a specimen with a 10^{o} edge notch, notch depth $a/w = 0.5$ and a stress- strain curve given by figure 14 were compared with experimental results obtained by Bubsey, R. T. and Jones, M. (ref. 10). The specimen used in this experiment, made of Al 5083-0 with length to width ratio of 4:1, crack length $a/w = 0.5$ was subjected to three point bending. The experimental results as shown in figure 15 are in good agreement with the numerical results obtained herein.

The product of y-directional stress and total strain was calculated for various cases. The order of singularity of that product was determined by plotting $\ln(\sigma_y \epsilon_y)$ versus $\ln r$ and by making a least squares fit of a straight line through the plotted points. It was found to be very close to unity.

Finally, Rice's J integral was evaluated for several cases by using relations given in reference 5. In these calculations, straight line paths were chosen through the plastic zone near the tip of the notch. The integral was evaluated using values of stresses, strains and displacements at cells centroids for a number of paths. The path-independence of J was not conclusive, since the results varied up to 15 percent from the averaged value. It is possible that the results obtained herein do not indicate that the path independent property is lost but rather that

the field values of the displacements are not calculated with sufficient accuracy.

The average values of the dimensionless J integral as a function of load are plotted in figure 16 for a case of a specimenn with a 10^{o} edge notch, a/w = 0.5, m = 0.05 and plane strain condition. At the start of plastic flow J increases rapidly with load. This is followed by almost linear variation with additional load.

The relations between the J integral and stress intensity factor K_I developed for linear elasticity are obviously not applicable for the elastoplastic problem. By plotting the dimensionless J/K_I^2 ratios as a funtion of load q, the relation between the J integral and the dimensionless stress intensity factor K_I is obtained. A typical plot is shown in figure 17. In all cases, the ratio J/K_I^2 remains almost equal to elastic value of 0.89 for plane strain or 1.0 for plane stress and increases sharply at the load corresponding to the appearance of the plastic zone at the boundary opposite the notch. Once the transition occurs the ratio increases approximately proportionally to the load increment.

CONCLUSIONS

The boundary integral equation method proved to be capable of giving very detailed results such as stress and strain distributions around the tip of the notch and, related to them, the shapes of plastic zones. This was accomplished using a relatively small number unknowns.

The obtained results also provide the information of the effect of strain hardening and on the differences that occur between plane stress and plane strain solutions. The order of singularity for the strain energy density was found to be unity, which is consistent with results previously obtained by other investigators.

The stress intensity factor was calculated for several cases. The path independence property of Rice's J integral was qualitatively confirmed and the relation between J and the stress intensity factor was graphically extended into the elastoplastic range.

The presence of a singularity at the tip of the notch makes accurate answers very difficult to obtain. Nevertheless good agreement was obtained between the calculated results and experimentally measured notch opening displacement as shown in figure 15. Some improvement in the solution techniques and further investigation of the influence of the boundary nodal spacing and interior grid size on the resulting stress and strain fields, and therefore, on the notch opening displacements and J integrals, may be desirable.

REFERENCES

1. Bowie, O.L.: Rectangular Tensile Sheet with Symmetric Edge Cracks. Appl. Mech., vol. 86, no. 2, June 1964, pp. 208-212.

2. Gross, Bernard: Some Plane Problem Elastostatic Solutions for Plates Having a V-Notch. Ph.D. Thesis,. Case Western Reserve Univ., 1970.

3. Hays. David J.: Some Applications of Elastic-Plastic Analysis to Fracture Mechanics. Ph.D. Thesis,. Imperial College of Science and Technology, Univ. London, 1970.

4. Mendelson, Alexander: Boundary Integral Methods in Elasticity and Plasticity. NASA TN-D-7418, 1973.

5. Rzasnicki, Walter; Mendelson, Alexander; and Albers, Lynn U.: Application of Boundary Integral Method to Elastic Analysis of V-Notched Beams. NASA TN-D-7424, 1973.

6. Swedlow, J.L.; and Cruse, T.A.: Formulation of Boundary Integral Equations for Three-Dimensionsl Elasto-Plastic Flow. Int. J. Solids Structures, vol. 7, 1971, pp. 1673-1683.

7. Swedlow, J.L.; Williams, M.L.; and Yang, W.H.: Elasto-Plastic Stresses and Strains in Cracked Plates. Presented at the 1st International Conference on Fracture, Sandai, Japan, 1965.

8. Mendelson, Alexander: Plasticity: Theory and Application. Macmillan Co., 1968.

9. Rzasnicki, Walter: Plane Elasto-Plastic Analysis of V-Notched Plate Under Bending by Boundary Integral Equation Method. Ph. D. Thesis, Univ. Toledo, 1973.

10. Bubsey, R.T.; and Jones, M.H.: Private Communications. NASA Lewis Research Center, Cleveland, Ohio, Nov. 1972.

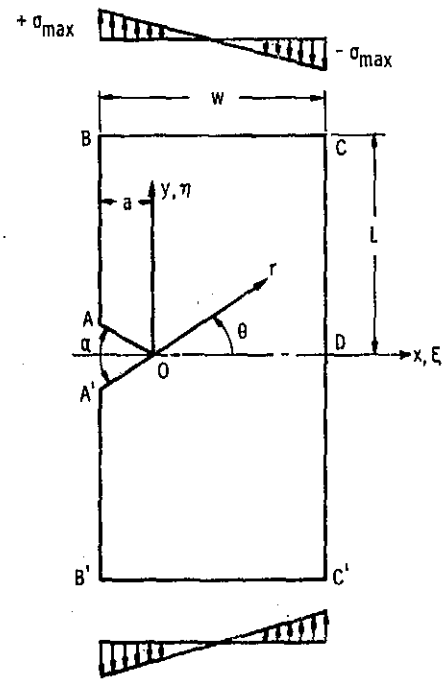

Figure 1. - Single-edge V-notched beam subject to pure bending load.

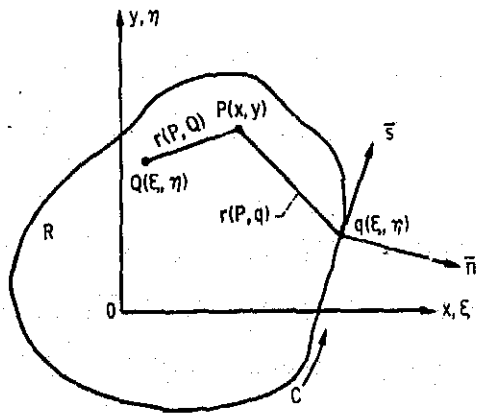

Figure 2. - Sign convention for a simply connected region R.

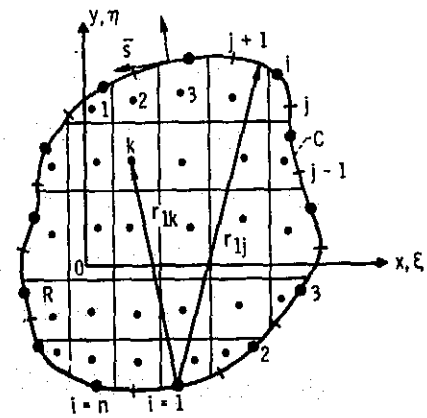

Figure 3. - Boundary and interior region subdivisions for P(x, y) ⊂ C.

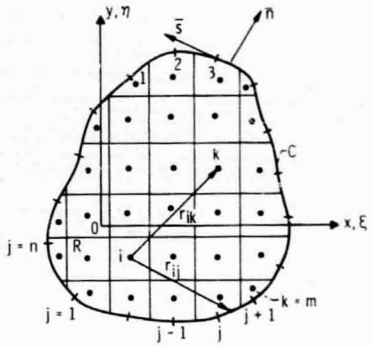

Figure 4. - Boundary and interior region subdivisions for P(x, y) ∈ R.

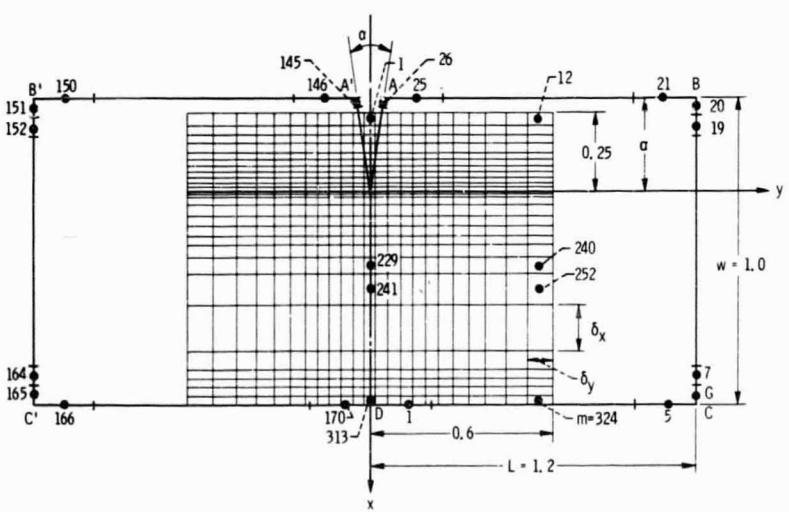

Figure 5. - Distribution of boundary subdivisions and typical interior grid for elastoplastic problem. All distances are made dimensionless with respect to beam width w.

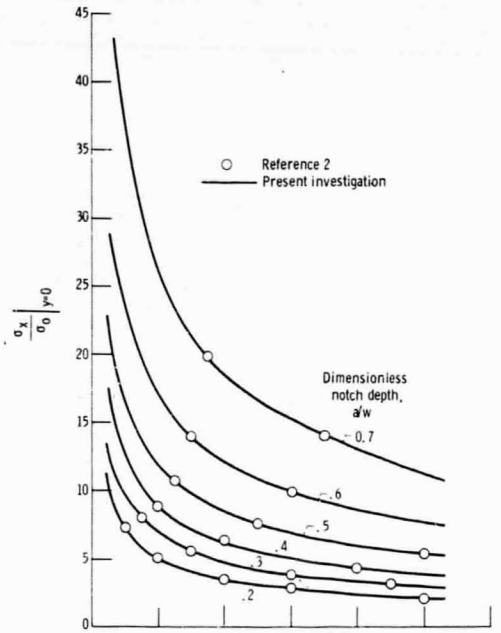

(a) Dimensionless x-directional stress as a function of x/w.

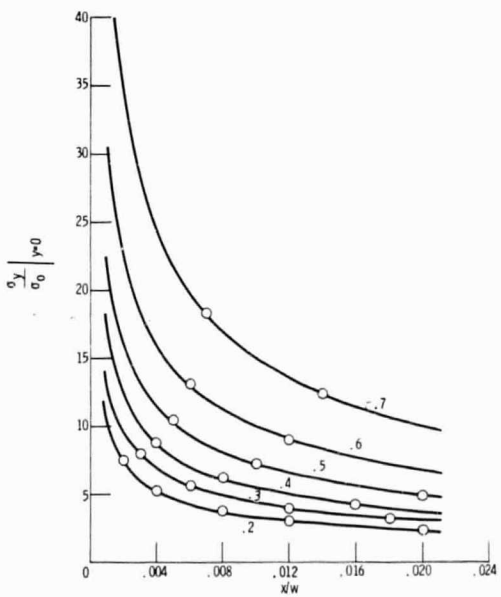

(b) Dimensionless y-directional stress as a function of x/w.

Figure 6. - Dimensionless elastic x-directional and y-directional stress distribution in the vicinity of the notch for a specimen with a 10^0 edge notch subjected to pure bending, $\sigma_{max}/\sigma_0 = 1$.

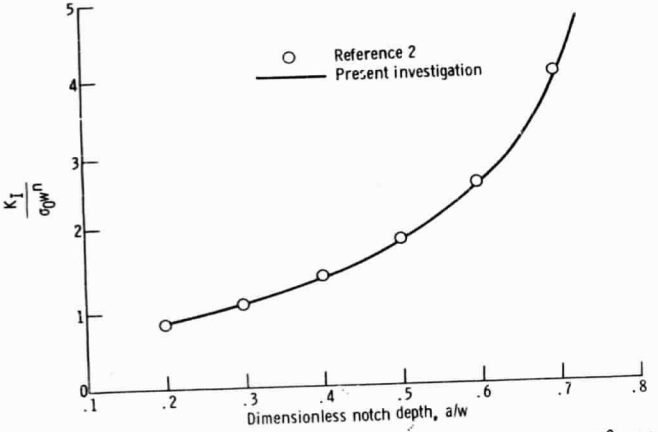

Figure 7. - Dimensionless stress intensity factor for a specimen with a 10^0 notch subjected to pure bending and behaving elastically, $\sigma_{max}/\sigma_0 = 1$.

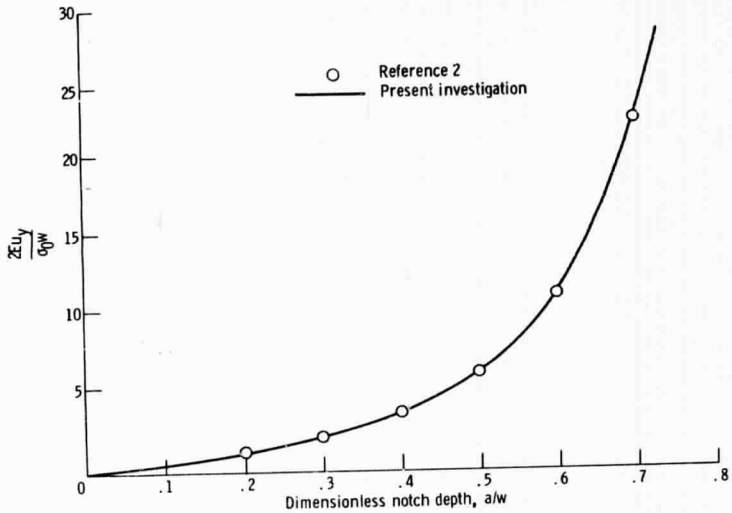

Figure 8. - Dimensionless elastic plane-stress y-directional notch opening displacement for a specimen with a 10^0 edge notch subjected to pure bending. Poisson's ratio $\mu = 0.33$, $\sigma_{max}/\sigma_0 = 1$.

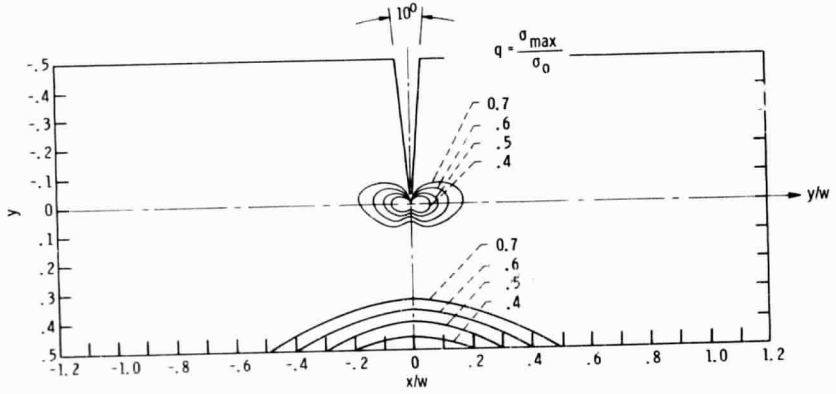

Figure 9. - Growth of the plastic zone size with load for a specimen with a 10^0 edge notch subjected to pure bending; plane strain a/w = 0.5, $\alpha = 10^0$, m = 0.05, $\mu = 0.33$

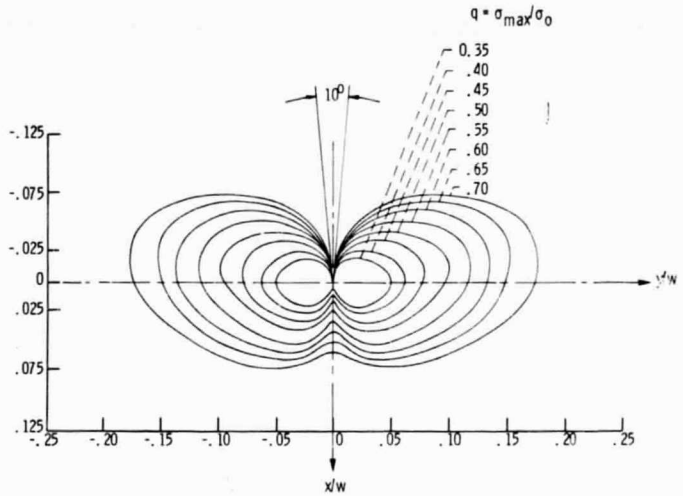

Figure 10. - Growth of the plastic zone size with load in the vicinity of the notch for a specimen with a 10^0 edge notch subjected to pure bending; plane strain, a/w = 0.5, $\alpha = 10^0$, m = 0.05, $\mu = 0.33$.

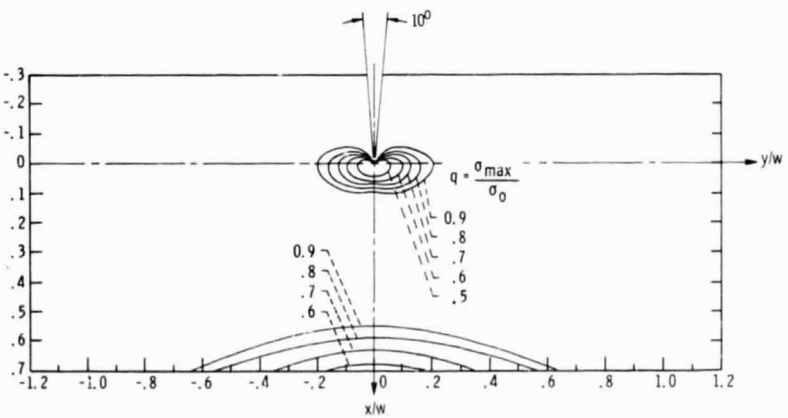

Figure 11. - Growth of the plastic zone size with load for a specimen with a 10^0 edge notch subjected to pure bending; plane stress, a/w = 0.3, $\alpha = 10^0$, m = 0.10, $\mu = 0.33$.

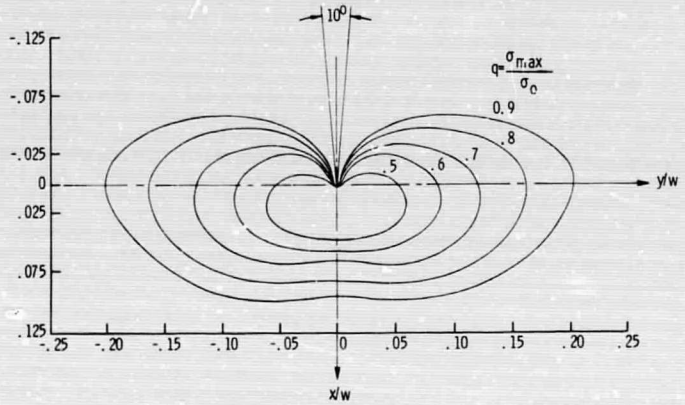

Figure 12. - Growth of the plastic zone size with load in the vicinity of the notch for a specimen with a 10^0 edge notch subjecyed to pure bending; plane stress a/w = 0.3, $\alpha = 10^0$, m = 0.10, μ = 0.33.

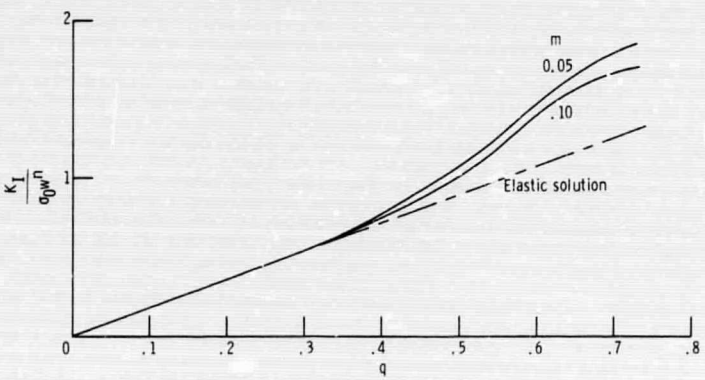

Figure 13. - Variation of dimensionless stress intensity factor with load for a specimen with a 10^0 edge notch subjected to pure bending; plane strain, a/w = 0.5, $\alpha = 10^0$, μ = 0.33.

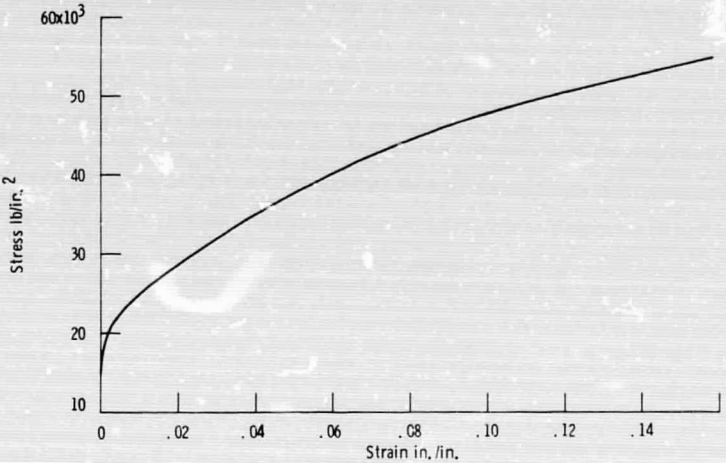

Figure 14. - Stress-strain curve for Al 5083-0 used in test (ref. (10)). $E = 11.3 \times 10^6$ lb/in.^{2}, $\mu = 0.33$.

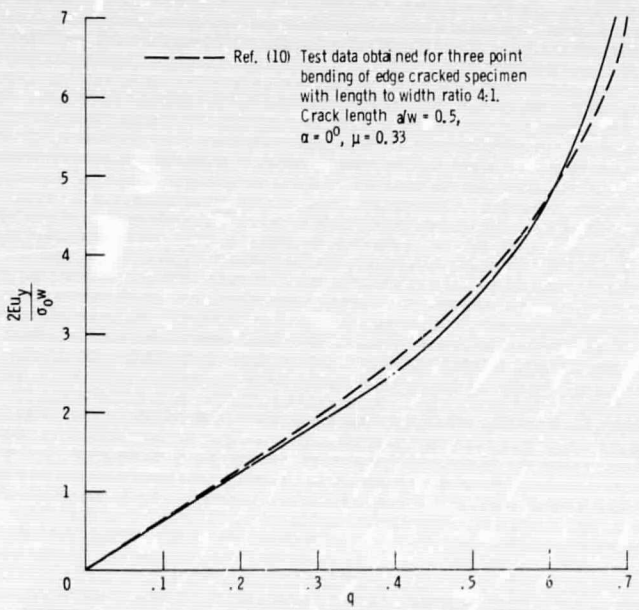

Figure 15. - Dimensionless plane strain y-directional notch opening displacement for a specimen with a 10° edge notch subjected to pure bending. a/w = 0.5, μ = 0.33.

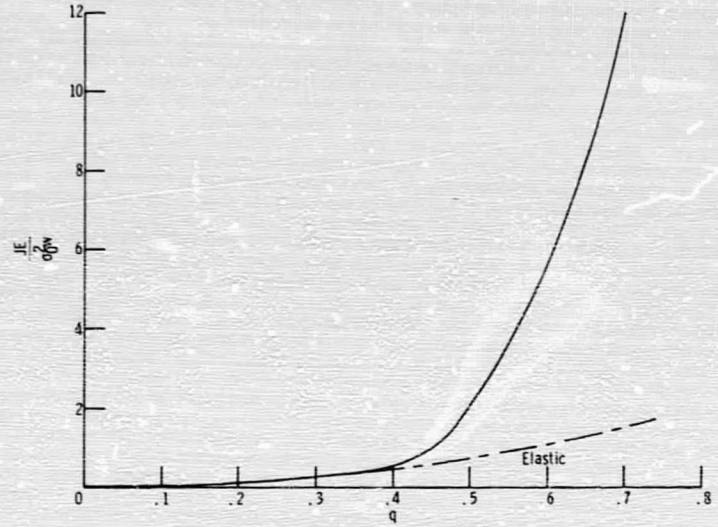

Figure 16. - Dimensionless plane strain J integral for specimen with a 10^0 edge notch subjected to pure bending; a/w = 0.5, $\alpha = 10^0$, m = 0.05, μ = 0.33.

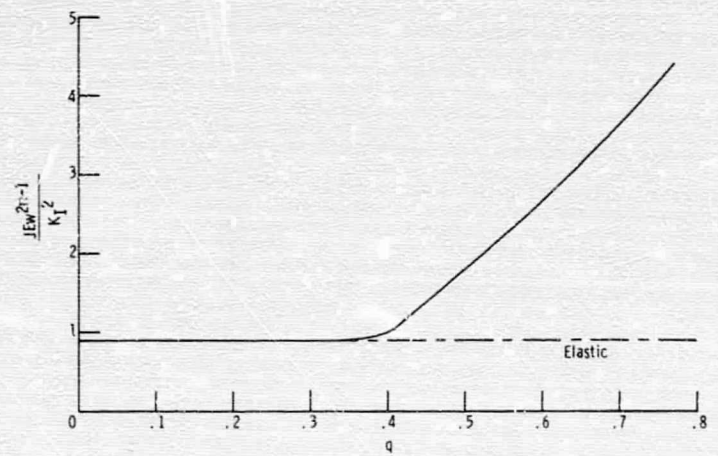

Figure 17. - Variation of the ratio of dimensionless J integral to the square of dimensionless stress intensity factor K_I^2 with load for a specimen with a 10^0 edge notch subjected to pure bending; plane strain, a/w = 0.5, $\alpha = 10^0$, m = 0.05, μ = 0.33.